THEORETICAL NOTES

Note 232

1 May 1975

SUB-SURFACE HEMP FIELD CALCULATION

by

G. H. Price

Stanford Research Institute

Menlo Park, California 94025

76-049

Sub-Surface HEMP Field Calculation

I INTRODUCTION

The electromagnetic pulse (EMP) interaction threat is nominally specified in terms of the free-space field. However, this specification is not always directly useful. Particularly in the case of buried structures, the field characteristics in the vicinity of the system are much modified from their free-space form. The objective here is to calculate the subsurface electric and magnetic fields corresponding to a nominal high-altitude EMP threat for a representative geometry.

II FREE-SPACE FIELD

The free-space electric field is taken to be

$$E(t) = E_o(1 - e^{-t/t_1})e^{-t/t_2} \tag{1}$$

with

$t_1 = 3.5\ \mu s$

$t_2 = 275\ \mu s$

$E_o = 50\ kV/m.$

The corresponding magnetic field is given by

$$H(t) = \frac{1}{Z_o} E(t) \tag{2}$$

where $Z_o = (\mu_o/\epsilon_o)^{\frac{1}{2}} = 377\ \Omega$ is the impedance of free space with μ_o the permeability and ϵ_o the permittivity of free space, respectively. These free-space fields are illustrated in Figure 1.

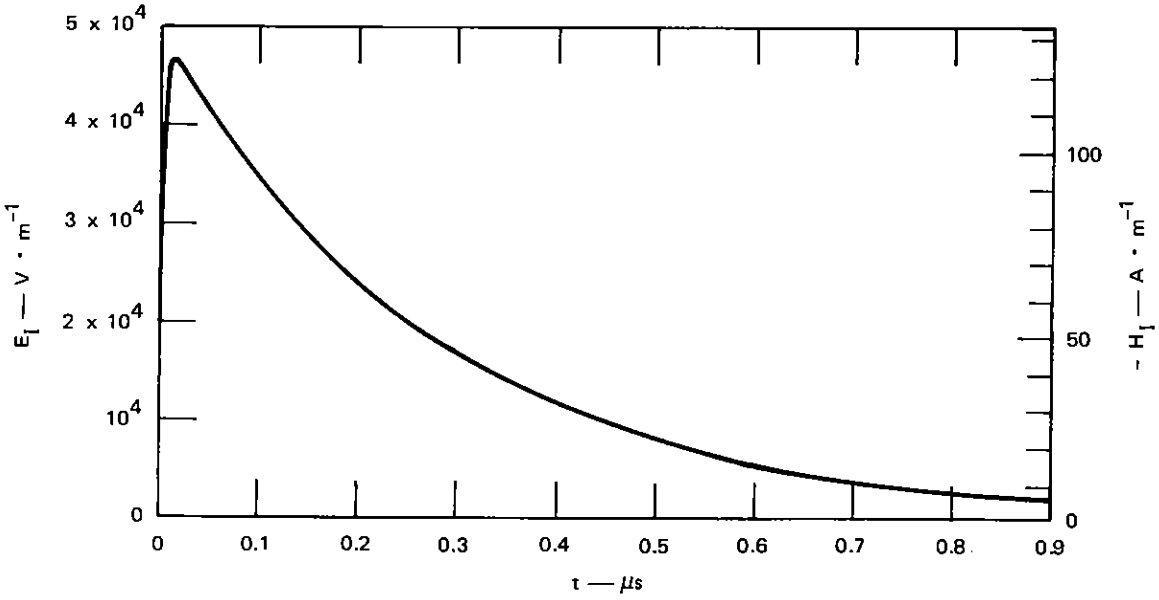

FIGURE 1 INCIDENT PULSE

III FIELDS IN THE EARTH

A. Formulation

The penetration of the incident pulse into the earth is modeled as a straight forward, planar reflection/transmission problem, as shown in Figure 2. The earth's surface is taken to be the plane $x = 0$, with $x > 0$ free space and $x < 0$ within the earth. The earth is assumed to be a homogeneous, lossy dielectric characterized by a conductivity σ, a permittivity ϵ, and a permeability equal to that of free space--$\mu = \mu_o$.

With this model, the field expressions for a time-harmonic incident wave are well known. For a wave of angular frequency ω, incident at an angle θ_o from the vertical (x axis) with its electric field parallel to the surface (i.e., transverse electric) the sub-surface electric field $\vec{E}_t(\omega)$ is given by[1]

$$\vec{E}_t(\omega) = \vec{E}_1(\omega) \exp(ik_1\vec{n}_1 \cdot \vec{r} - i\omega t) \qquad (3)$$

[1] J. A. Stratton, Electromagnetic Fields, (McGraw-Hill Book Company, New York, 1941).

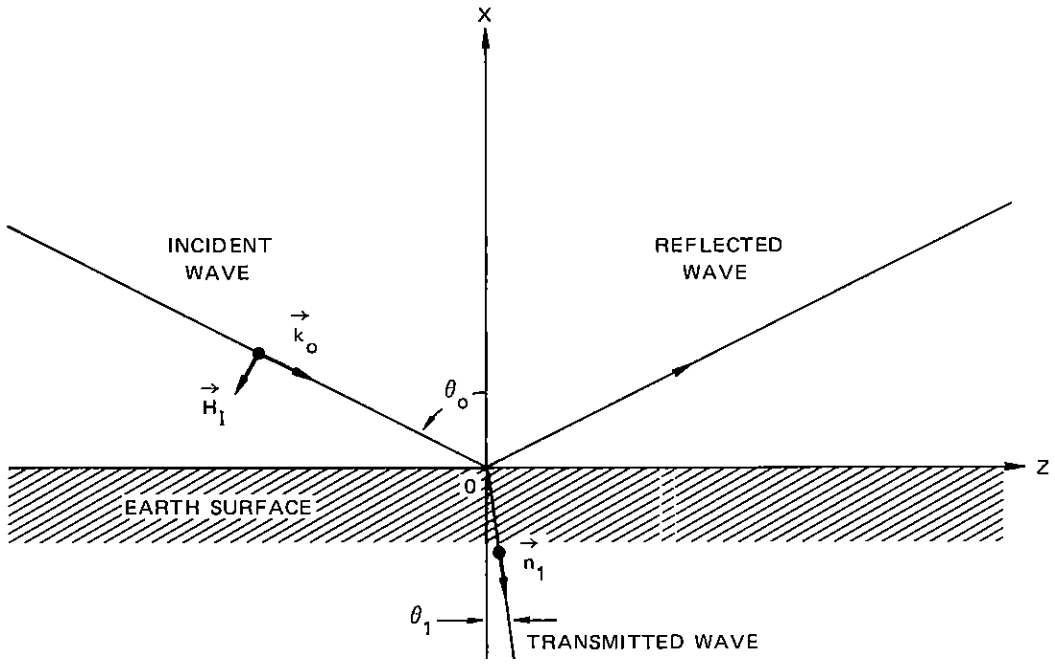

FIGURE 2 GEOMETRY

with

$$\vec{E}_1(\omega) = \frac{2\cos\theta_o}{\cos\theta_o + \left[\left(\frac{k_1}{k_2}\right)^2 - \sin^2\theta_o\right]^{1/2}} \vec{E}_i(\omega) \ . \tag{4}$$

The wave numbers k_1 and k_2 are given by

$$k_1 = \left(\frac{\epsilon}{\epsilon_o} - \frac{\sigma}{i\omega\epsilon_o}\right) k_o \tag{5a}$$

$$k_2 = k_o = \frac{\omega}{c} \ , \tag{5b}$$

where c is the speed of light in free space. The subscripts 1 and 2 denote the regions within the earth and in free space, respectively.

The vector $\vec{n}_1$ is a unit vector in the direction of the wave normal within the earth, at an angle θ_1 relative to the negative x axis; this direction is determined by Snell's law

$$k_1 \sin \theta_1 = k_o \sin \theta_o \ . \tag{6}$$

Since k_1 is complex, so is θ_1, and $\vec{n}_1 \cdot \vec{r}$ has both real and imaginary components, describing the phase and amplitude variation, respectively, of the wave within the earth. If the electric field in the incident pulse is taken to be parallel to the y axis, $\vec{n}_1$ lies in the x - z plane and

$$\vec{n}_1 \cdot \vec{r} = - x \cos\theta_1 + z \sin\theta_1 \ . \tag{7}$$

The spectral components $\vec{E}_i(\omega)$ are given by the Fourier transform of the incident pulse. With our choice of the incident electric field parallel to the y axis,

$$\vec{E}_i(\omega) = \hat{i}_y \int_o^\infty dt \ e^{i\omega t} \ E(t) \ , \tag{8}$$

where $\hat{i}_y$ is a unit vector parallel to this axis. The integral is readily evaluated analytically for the E(t) given by Eq. (1), to give

$$E_i(\omega) = E_o \left(\frac{t_2}{1 - i\omega t_2} - \frac{t_c}{1 - i\omega t_c} \right) \tag{9}$$

where

$$t_c = \frac{t_1 t_2}{t_1 + t_2} \ . \tag{10}$$

The magnetic field within the earth is given in terms of $\vec{E}_t$ and $\vec{n}_1$ by

$$\vec{H}_t(\omega) = \frac{k_1}{\mu_o \omega} \vec{n}_1 \times \vec{E}_t \ . \tag{11}$$

Explicitly, Eq. (11) can be worked through to obtain

$$H_{t_x} = - \frac{E_t}{Z_o} \sin\theta_o \tag{12a}$$

$$H_{t_z} = - \frac{E_t}{Z_o} \left[\left(\frac{k_1}{k_2} \right)^2 - \sin^2\theta_o \right]^{1/2} \tag{12b}$$

where E_t is given by Eq. (3).

B. Results

The above equations have been used to calculate the sub-surface electric and magnetic fields in typical soil, $\sigma = 3 \times 10^{-3}$ mho $\cdot$ m^{-1} and $\epsilon = 10\ \epsilon_o$, for a pulse obliquely incident upon the earth's surface at an angle $\theta_o = 70°$. The magnitude of the spectral components $E_t(\omega)$ and $H_t(\omega)$ are shown in Figure 3 at depths of 0, 10, and 20 m, along with those of the incident electric field calculated from Eq. (9). The magnetic field, H_t, is elliptically polarized; that is, the magnetic field vector $\vec{H}_t(\omega)$ rotates in the x - z plane with its tip tracing out an ellipse. The magnitude of the major semi-axis of this ellipse (which lies nearly parallel to the z axis for our example) has been plotted in Figure 3 to represent H_t. The scales of the E and H axes have been deliberately chosen to produce the coalescence of the E and H spectra seen at the high frequencies.

The time-domain fields corresponding to these spectra are shown in Figure 4. Since the major semi-axis of the H_t ellipse does not lie in a fixed direction as a function of frequency, the major component of $\vec{H}_t$, $H_H = - H_{t_z}$, has been Fourier transformed to give the magnetic fields shown in Figure 4. The onset of the field is increasingly delayed with increasing depth beneath the surface as a result of the time required for the field to propagate to that depth. The time origin has been taken to correspond to the onset of the incident pulse at the point on the surface vertically above the field-observation point.

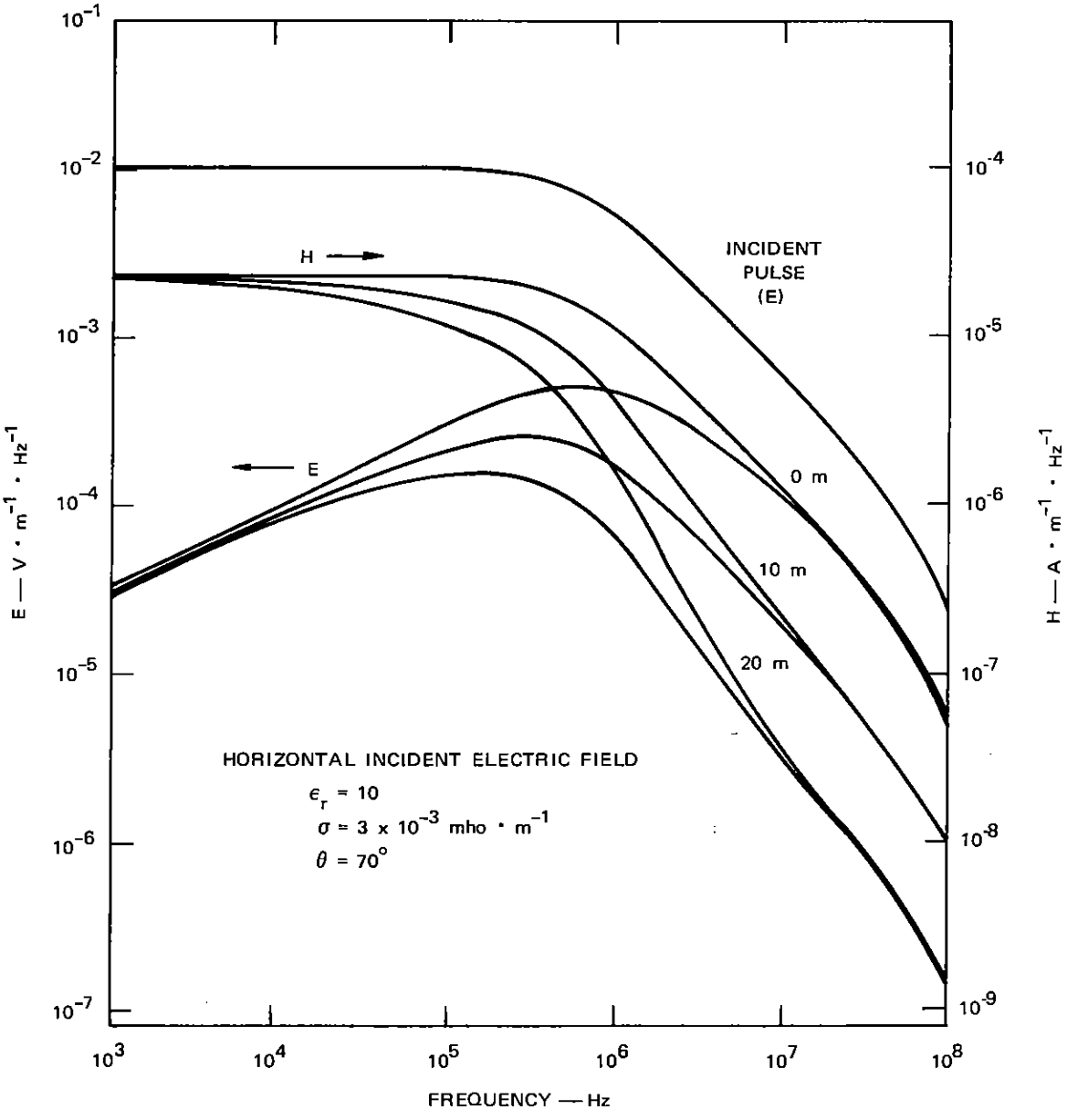

FIGURE 3 SPECTRA OF ELECTRIC AND MAGNETIC FIELDS AT VARIOUS DEPTHS

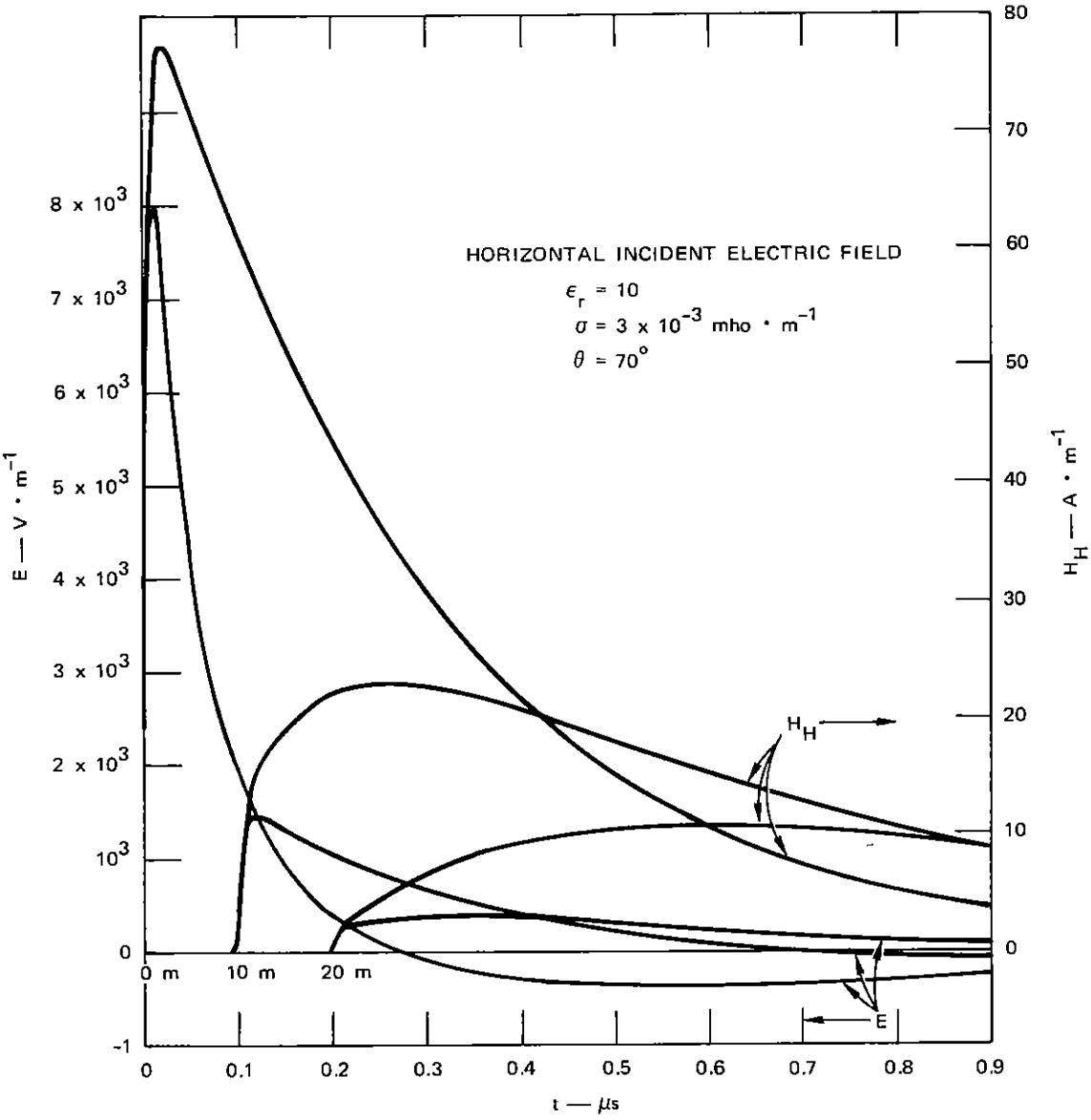

FIGURE 4 ELECTRIC AND MAGNETIC FIELDS AT VARIOUS DEPTHS

The greater loss beneath the surface of the low-frequency spectral components in E relative to those in H that is evident in their spectra, Figure 3, is also apparent when their waveforms are compared for a given depth. The H_H waveforms consistently show a later and less sharp peak than do those for E. Also evident in both E and H waveforms is the progressive loss of the higher-frequency spectral components with increasing depth. This loss is manifest both in the increasing delay of the field peak and in the reduced slope of the initial field buildup with increasing depth. This last behavior is shown in greater detail in Figures 5, 6 and 7 in which E and H_H are plotted individually.

The reduction in the initial rate of change (slope) of the fields with increasing depth is of particular interest for the magnetic field since its coupling effectiveness tends to be proportional to dH/dt. In order to provide a more quantitative measure of the reduction of dH/dt with increasing depth, the spectra of H_H were modified (by multiplication by $-i\omega$) and inverse transformed to give $dH_H(t)/dt$. The peak values of dH_H/dt scaled from these waveforms are given in Table 1 as fractions of the peak dH/dt in the incident pulse. As can be seen from the table, the reduction in dH/dt beneath the surface is indeed marked. It should also be noted that the reduction in dH/dt is appreciable even at the surface. Since the horizontal magnetic field must be continuous across the surface, this reduction is also relevent to unburied systems located on the surface.

Table 1

Peak Rate of Change of Magnetic Field Relative to that in Incident Pulse	
Depth (m)	$(dH_H/dt)_{peak}/(dH_I/dt)_{peak}$
0	0.174
10	0.029
20	0.005

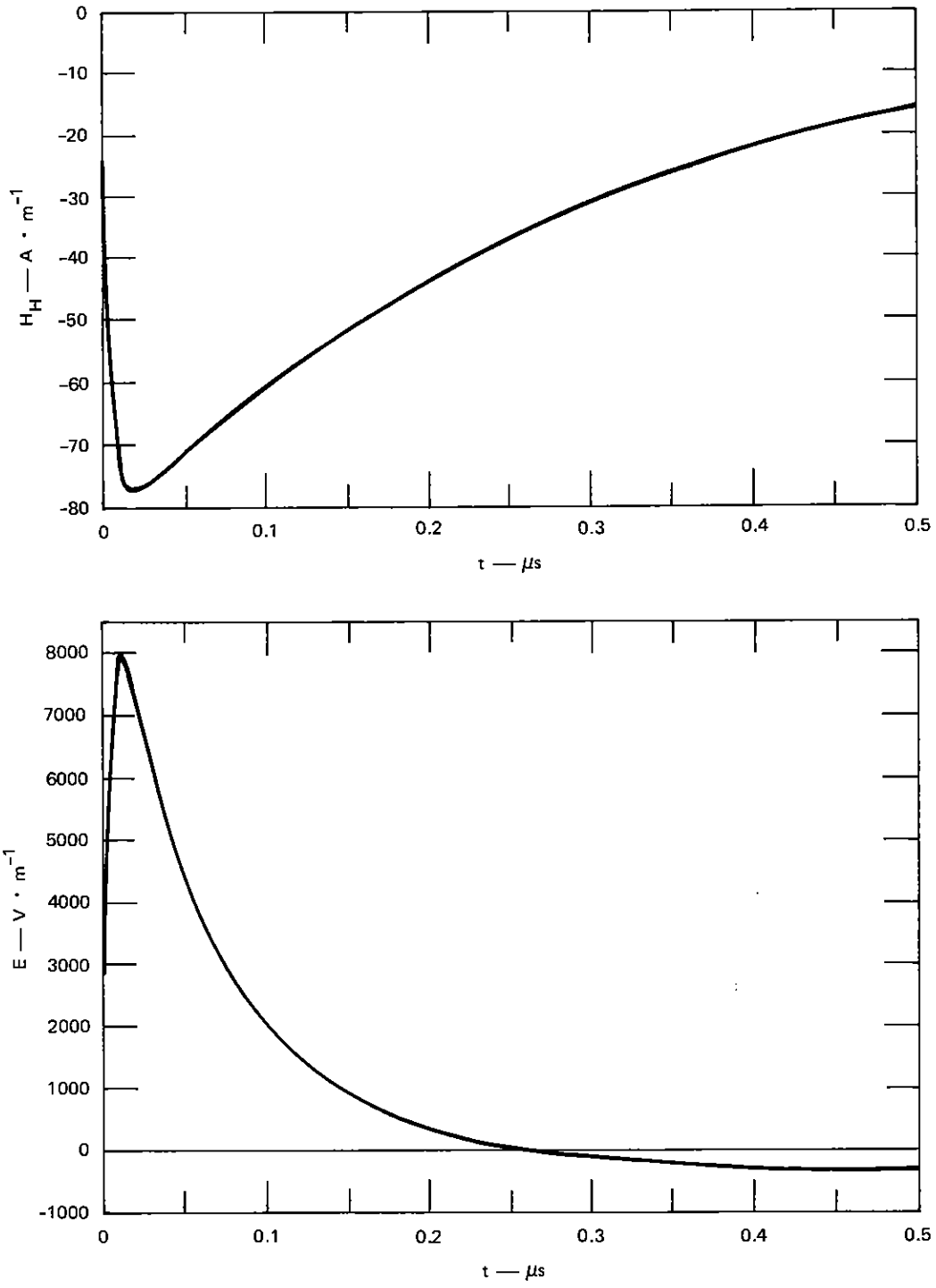

FIGURE 5 HORIZONTAL MAGNETIC AND ELECTRIC FIELDS AT 0 m (surface)

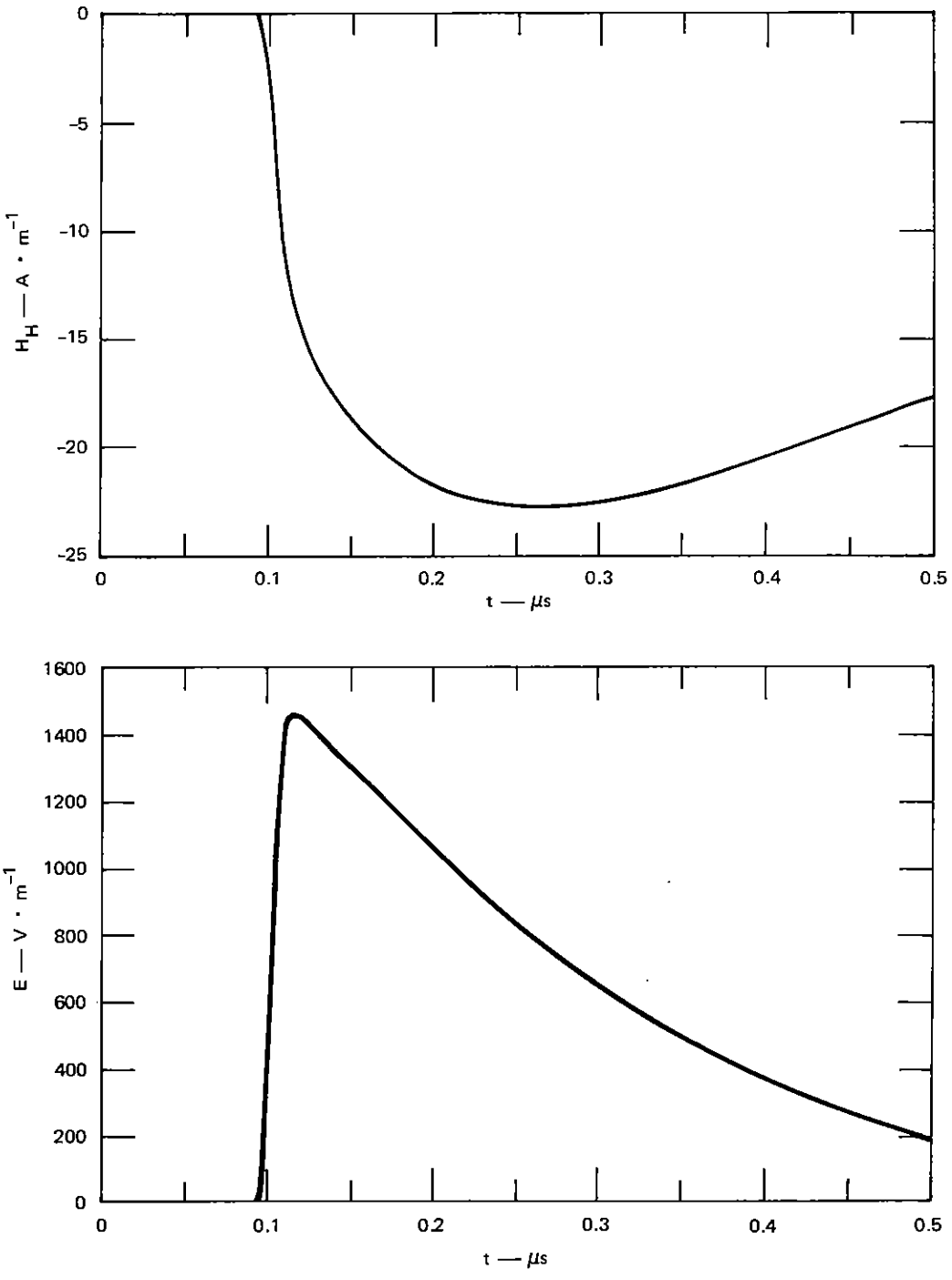

FIGURE 6 HORIZONTAL MAGNETIC AND ELECTRIC FIELDS AT 10 m DEPTH

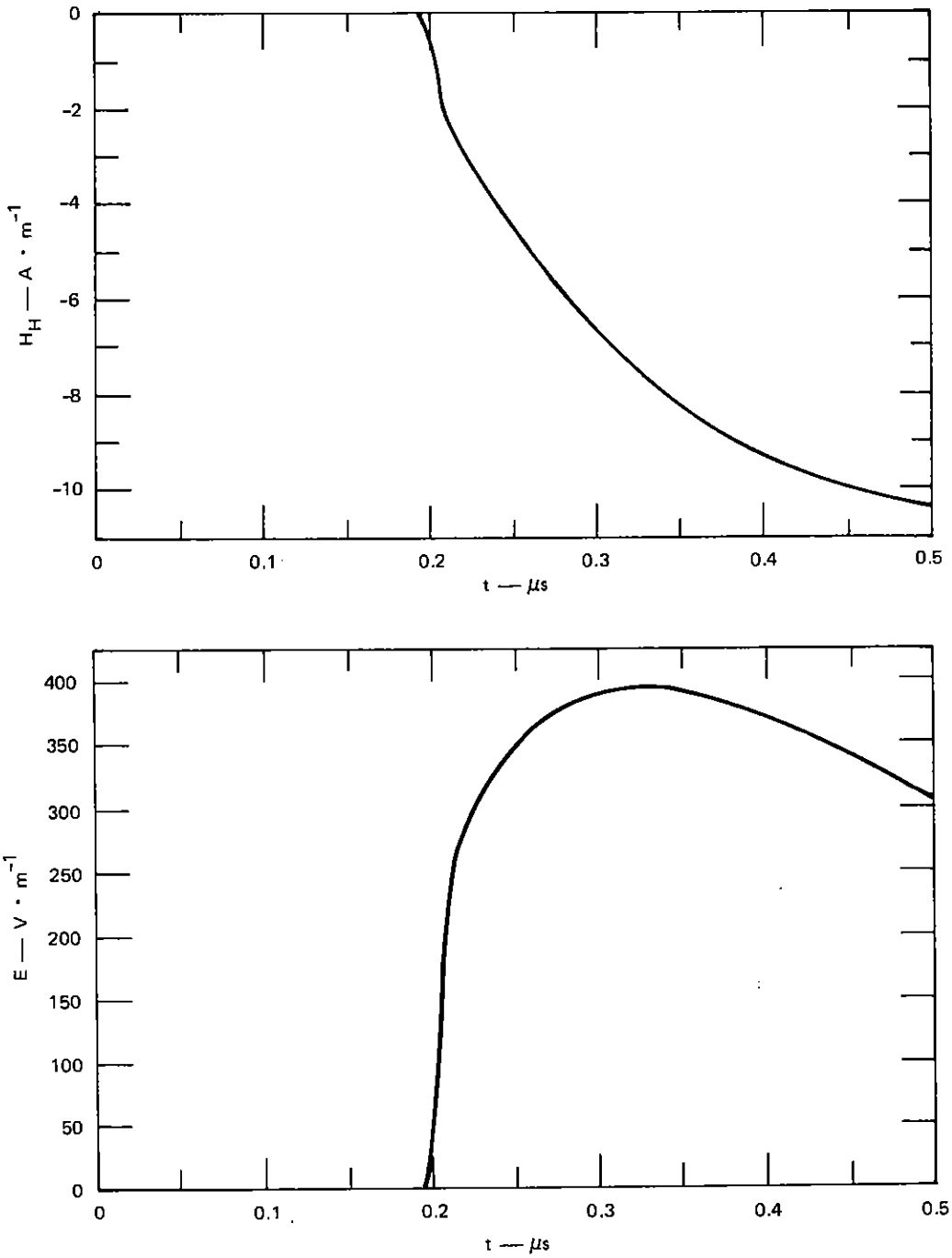

FIGURE 7 HORIZONTAL MAGNETIC AND ELECTRIC FIELDS AT 20 m DEPTH